High-brilliance Zeeman-slowed cesium atomic beam

F. Lison, P. Schuh, D. Haubrich, and D. Meschede
Institute for Applied Physics, University Bonn, Wegelerstrasse 8, D-53115 Bonn, Germany
(Received 9 April 1999; published 10 December 1999)

We have built a Zeeman-slower apparatus which produces a slow and cold cesium atomic beam. The atomic beam has a mean velocity in the range 35–120 m/s and a high atomic current of more than 2×10^{10} cold atoms/s. A small longitudinal velocity spread was achieved by optimizing the termination of the slowing process. The measured value of less than 1 m/s is consistent with a numerical simulation of the slowing process. With a magnetic lens and a tilted two-dimensional optical molasses stage, the slow atomic beam is transversely compressed, collimated, and deflected. We achieve a transverse temperature below the Doppler limit. The brilliance of this beam has been determined to be 7×10^{23} atoms $s^{-1}m^{-2}$ sr^{-1}. By optical pumping the slow atomic beam can be polarized in the outermost magnetic substates $F=4,m_F=\pm4$, of the cesium ground state. This brilliant beam is an ideal source for experiments in atom optics and atom lithography.

PACS number(s): 32.80.Pj, 42.50.Vk

INTRODUCTION

Atomic beams provide an extremely versatile and useful tool for many precision experiments. However, in many applications the necessity of a high degree of collimation leads to a significant loss of atomic flux. Furthermore, transit time broadening due to the high mean velocity in the beam limits the achievable resolution. Laser cooling has overcome these limitations, and several sources of slow and cold atomic beams have been designed and investigated. For instance, from a variant of the magneto-optical trap (MOT) atoms can routinely be extracted at low velocities and with a reasonably small velocity spread [1]. However, for many applications in atom optics, such as atom lithography, high flux atomic beams with moderate velocities (50–100 m/s) are desirable, because collisions with residual gas molecules become increasingly important at low velocities with their long travelling times. These requirements are met by the Zeeman slowing technique [2], which produces a continuous flux of slow and cold atoms. In this paper we will show that it allows to produce 2.6×10^{10} cold atoms s^{-1} in a continuous beam with a brilliance of 7×10^{23} atoms s^{-1} m^{-2} sr^{-1}.

I. CHARACTERIZATION OF ATOMIC BEAMS

A. Thermal atomic beams

The properties of a thermal atomic beam are completely defined by the temperature of its source and the apertures used to shape it. We assume an isotropic flux density $\Phi_S=I_S/\pi(\Delta x_S)^2$ of atoms emanating from a source aperture. The brightness (see the Appendix for a definition) after a second aperture with extension $\pi(\Delta x_A)^2$ placed at a distance L from the source is given by

$$\mathcal{R}_A\approx\frac{I_A}{\pi^2(\Delta x_A)^2[(\Delta x_A+\Delta x_S)/L]^2}=\frac{I_S}{4\pi^2(\Delta x_A+\Delta x_S)^2}, \tag{1}$$

where we used $I_A=I_S(\Delta x_A)^2/4L^2$, and expressed the solid angle by the collimation ratio. Note that for a given current from the source I_S the brightness no longer depends on the separation L, in accordance with Liouville's theorem. For a negligible source aperture ($\Delta x_S/\Delta x_A\ll1$), Eq. (1) describes the brightness of a point source.

To illustrate the order of magnitude involved, let us consider our thermal cesium atomic beam with a flux density of 1.4×10^{10} atoms s^{-1} mm^{-2} and a collimation ratio of 1:150 effusing from an oven with a temperature of $T=410$ K. This beam has a brightness of $\mathcal{R}\simeq10^{20}$ s^{-1} m^{-2} sr^{-1}, and the dimensionless phase space density is given by $\tilde{\Lambda}\simeq10^{-15}$.

B. Laser-cooled atomic beams

Laser-cooling techniques enable to increase the phase space density of atomic beams. Transverse laser cooling increases the brightness and brilliance, whereas longitudinal cooling only enhances the brilliance.

Transverse laser cooling of atomic beams is easily implemented and frequently used [3,4]. It reduces the angular divergence of the beam ($\Delta\Omega$) without loss of current. The brightness can be further improved by reducing the beam cross section $\pi(\Delta x_\perp)^2$. This has been demonstrated using a two-dimensional magneto-optical trap [5,6]. Longitudinal laser cooling is more difficult to achieve because for both the Zeeman slowing as well as the chirp slowing technique [7], a longitudinal superposition of the atomic beam and the slowing laser beams is necessary. For useful instrumentation a separation of the slowed beam from the slowing axis is required, increasing the technical complexity of the apparatus.

A convenient device derived from a magneto-optical trap for the production of a slow beam was demonstrated by Lu *et al.* [8]. This variant serves as a continuous source of cold atoms with high brightness, brilliance, and phase-space densities. Figure 1 presents a collection of brightness and brilliance values for different atomic beam sources that can be found in the literature. Applications such as atom lithography not only require a high flux density, but also high current and a high ratio of $\overline{p_\parallel}/\Delta p_\parallel$ to warrant focusing properties. In our opinion, these requirements are best fulfilled by the Zeeman slowing technique.

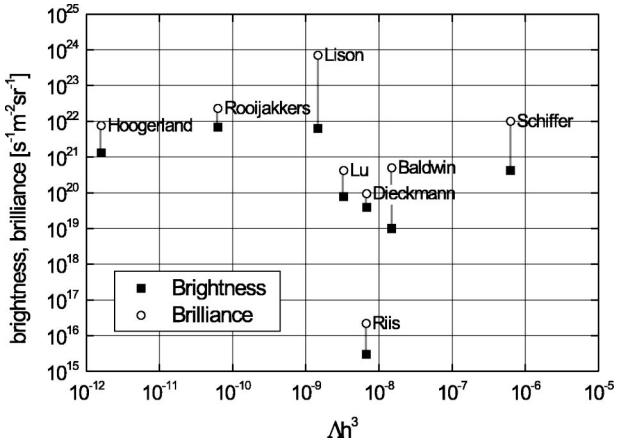

FIG. 1. Phase-space density, brightness, and brilliance for several atomic beam sources. Metastable rare-gas sources: Hoogerland *et al.* [18], Schiffer *et al.* [24], Rooijakkers *et al.* [25], and Hoogerland *et al.* [26]. Alkali sources: Dieckmann *et al.* [1], Riis *et al.* [5], Lu *et al.* [8], and Lison (this work).

II. ZEEMAN SLOWING

In a Zeeman slower a fixed-frequency laser counterpropagates the atomic beam and decelerates the atoms by resonant radiation pressure. The change in detuning caused by the Doppler effect during the deceleration process is compensated for by an inhomogenous magnetic field superimposed on the slowing axis. In order to achieve nearly constant deceleration in a tapered magnetic solenoid extending from $z=0$ to z_S, the field strength on axis must obey the relation

$$B(z)=B_0+B_1\sqrt{1-z/z_S}. \tag{2}$$

For a given length z_S and deceleration a_S, only atoms with an initial velocity v smaller than the maximum capture velocity

$$v_S=(2a_Sz_S)^{1/2} \tag{3}$$

can be brought to a stop. The deceleration a of an atom with mass m is given by

$$a=\frac{\hbar k\Gamma}{2m}\frac{s_0}{1+s_0+(2\Delta/\Gamma)^2}, \tag{4}$$

where $\lambda=2\pi/k$ is the wavelength of the transition, Γ is the natural decay rate of the excited state, and $s_0=I/I_0$ the normalized intensity. The detuning is given by $\Delta=\omega_{\mathrm{Laser}}-\omega_{\mathrm{Atom}}-\mu B(z)/\hbar+kv$. To keep the atoms in resonance during the slowing process, the change in detuning due to the varying magnetic field must not exceed the changing Doppler shift

$$\mu\frac{dB}{dz}v(z)\leqslant\hbar ka. \tag{5}$$

A detailed theoretical description of the dynamics of the slowing process was given in Refs. [9] and [10], and we adopt the notation of Ref. [10]. The key feature of these

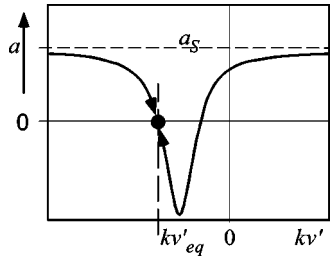

FIG. 2. Velocity dependence of the acceleration in a decelerated reference frame. The residual velocity is damped to the equilibrium value at v'_{eq}.

treatments is the transformation of the atomic equation of motion to a reference frame slowing at the design deceleration $a_S=dv_R/dt$. This leads to the equation of motion

$$\frac{d}{dt}v'=-\frac{\hbar k\Gamma}{2m}\frac{s_0}{1+s_0+(2(\Delta'+kv')/\Gamma)^2}-a_S \tag{6}$$

for the atomic velocity $v'=v-v_R$ in this reference frame, where $\Delta'=\omega_{\mathrm{Laser}}-\omega_{\mathrm{Atom}}-\mu B_0/\hbar$. A graphical illustration of the velocity dependence of dv'/dt shows the existence of a stable equilibrium at v'_{eq} associated with damping forces for cooling (Fig. 2). The predicted width of the longitudinal velocity distribution during the slowing process is comparable with the one-dimensional (1D) Doppler limit

$$\Delta v_{\mathrm{Doppler}}=\sqrt{\hbar\Gamma/m}=0.12\ \ \mathrm{m/s} \tag{7}$$

for cesium.

In order to extract an atomic beam with finite velocity from the Zeeman slower, it is necessary to terminate the slowing process by violating the condition of Eq. (5). Otherwise the atoms are brought to a stop or even sent back in the declining magnetic field. To also maintain the small longitudinal velocity spread of Eq. (7) the slowing process must be terminated abruptly. This is difficult to achieve in a standard σ^+ Zeeman slower, because the curvature of the decreasing magnetic field that can be obtained at the end of the solenoid is limited for technical reasons. Atoms then are initially tuned even more into resonance, and scatter many photons which leads to a heating of the atomic ensemble.

This problem can be overcome, however, by using an increasing magnetic field in combination with σ^--polarized light [11], or by the method which is conceptually shown in Fig. 3 for qualitative understanding and was used also by Molenaar *et al.* [10]: If the magnetic field is shaped as indicated in Fig. 3(b), the atoms are first tuned further out of resonance, and a steeper gradient of the magnetic field can be provided when the atom is transiting the resonance condition, dramatically reducing the number of scattered photons. We have investigated this termination process in detail, and compare the experimental results with a numerical simulation of the slowing process in Sec. V.

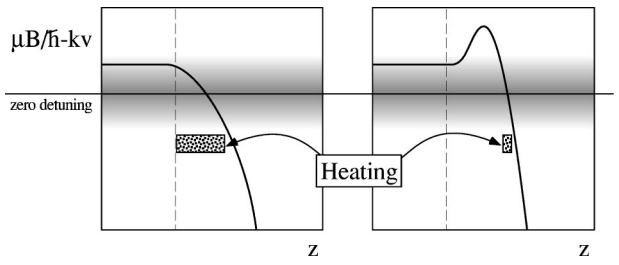

FIG. 3. Cooling of the σ^+ Zeeman cooler terminates at the dashed vertical line. A constant Doppler shift can be assumed beyond this point. Solid line: Zeeman tuned atomic frequency. Shaded area: Photon scattering rate. The heating period is much shorter for the right-hand configuration.

III. EXPERIMENTAL REALIZATION

A sketch of our experimental setup is shown in Fig. 4. The experiment uses altogether seven laser diodes (Spectra Diode Labs laser diodes with 50- and 100-mW output power) at 852 nm in the extended cavity design [12]. As a frequency reference we have set up a ''master'' diode laser. This is stabilized to the center of the cesium $F=4\rightarrow F'=5$ transition measured by polarization spectroscopy in a cesium vapor cell. The rms linewidth of this master laser with respect to the center of the atomic transition is determined from the error signal to be 500 kHz.

The cesium atomic beam effuses from a resistively heated stainless-steel cylinder through a 2-mm-diameter aperture, and is collimated by a second aperture (diameter 3 mm) 383 mm downstream. For an oven temperature of 140 °C, an absorption measurement results in a current value of $(1\pm0.1)\times10^{11}$ atoms s^{-1}, which is about a factor of 4 lower than theoretically expected. The inevitable expansion of the thermal atomic beam with a mean longitudinal velocity of 302 m/s to a diameter of about 20 mm at the end of the 1.4-m long slowing stage proved to be problematic for the slowing process. Therefore we installed a transverse optical collimation stage between the oven chamber and slowing region. An additional aperture (diameter 2 mm) is inserted between oven and collimation zone, which reduces the transverse velocity of atoms as well as the gas load (Fig. 4).

The molasses light field is provided by an elliptically shaped laser beam ($2w_x=5$ mm and $2w_z=45$ mm) folded around the atomic beam axis and retroreflected with the polarization of the light beams chosen to result in a lin. $\perp$ lin. configuration [13]. A repumping laser tuned to the $F=3\rightarrow F'=4$ transition with a power of 400 μW is added, which makes the fraction of atoms in the thermally populated $F=3$ ground state (7/16) accessible to the collimation process. The cooling laser frequency is tuned about two natural linewidths below the $F=4\rightarrow F'=5$ cooling transition. With a laser power of 24 mW the resulting velocity capture range $v_{\mathrm{cap}}\approx\Gamma\sqrt{1+s}/k=4.5\sqrt{1+s}$ m/s is larger than the maximum transverse velocity of atoms in the atomic beam. However, the velocity damping time for two-dimensional Doppler cooling [14] is on the order of 1 ms, which means only atoms with a longitudinal velocity of less than 50 m/s can be cooled toward their final transverse temperature. Fortunately, polarization gradient cooling mechanisms [13,15] which are present in our light field configuration lead to shorter damping times and hence more efficient cooling.

The beam diameter of the unslowed but collimated atomic beam of about 3 mm full width at half maximum (FWHM) at the end of the slowing region shows that the transverse velocity spread is reduced below the Doppler limit, resulting in a divergence of only 0.5 mrad. Although the total thermal beam current I is increased by only a factor of 2 to about 2×10^{11} atoms s^{-1} the current of the slowed and deflected atomic beam is increased by a factor of 20, as will be shown in Sec. IV C. The transverse cooling stage increases the brightness of the thermal atomic beam to $\mathcal{R}\simeq4\times10^{22}$ s^{-1} m^{-2} sr^{-1}, and the dimensionless phase space density of this beam is given by $\tilde{\Lambda}\simeq4\times10^{-13}$.

The magnetic field for Zeeman tuning of the resonance frequency varies approximately according to Eq. (2). It is produced by two coils (bias field B_0 and gradient field B_1) wound on a 38-mm inner diameter vacuum tube which is surrounded by a water cooling section. The bias field of $B_0=22$ mT reduces unwanted transitions into excited states decaying into the uncoupled $F=3$ ground state, which would terminate the slowing process. Figure 5 shows the measured magnetic-flux density on the atomic beam axis. Strong permanent magnets attached at the end of the slowing stage produce a large magnetic-field gradient which violates the adiabatic condition given in Eq. (5), and leads to a well-defined termination of the slowing process. The stray field of

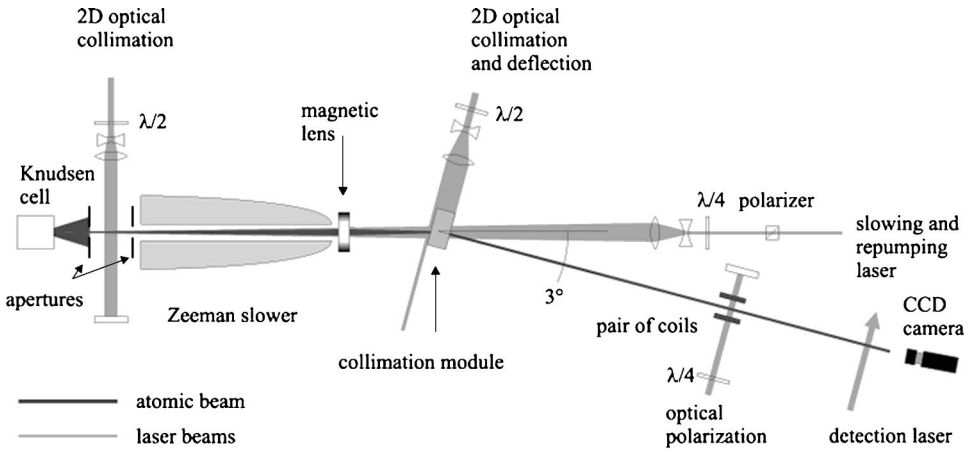

FIG. 4. Experimental setup of the Zeeman slower. The overall length is about 4 m.

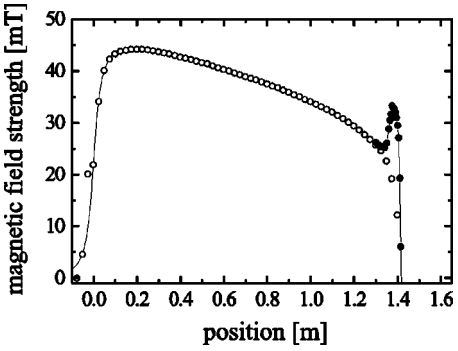

FIG. 5. Magnetic-flux density on the axis of the Zeeman slowing stage. Open dots without, full dots with termination field.

the Zeeman slowing magnet is nulled in the transverse collimation stage to less than 100 μT.

The slowing laser is a 100-mW laser diode frequency stabilized to the master laser by a standard phase-locking technique [16]. This allows us to control the detuning of the slowing laser with respect to the undisturbed $F=4\rightarrow F'=5$ transition over a large frequency range with radio-frequency precision, while preserving the small linewidth determined by the master laser. A polarization-preserving single-mode fiber guides the slowing laser beam to the experiment, where up to 32 mW of laser power are available. The laser beam is circulary polarized, expanded, and collimated with a telescope and superimposed onto the atomic beam axis. At the end of the slowing stage the laser beam diameter ($1/e^2$) is about 2.6 cm.

Though almost all atoms leave the collimation stage in the $F=4$ ground state, various atomic transitions decaying into the $F=3$ ground state become resonant with the slowing laser in the increasing magnetic field at the beginning of the slowing stage. This leak is closed by a repumping laser superimposed onto the slowing laser before both are coupled into the optical fiber. The repumping laser is stabilized onto an absorption spectrum in a cesium cell, and the available output power of about 350 μW is sufficient to repump almost all of the atoms back to the $F=4$ ground state.

The longitudinal slowing process introduces transverse heating resulting in a transverse velocity spread of the beam of

$$\Delta v_\perp \simeq \sqrt{\alpha v_{\mathrm{rec}} v_S}, \tag{8}$$

where $v_{\mathrm{rec}}=\hbar k/m=3.5$ mm/s is the recoil velocity for cesium, and the factor $\alpha=3/10$ accounts for the dipole pattern characteristic in the transverse direction. In our case the maximum velocity difference between initial and final velocity is $v_S\simeq 230$ m/s, corresponding to a transverse velocity spread of $\Delta v_\perp \simeq 0.35$ m/s. Associated with this effect is an increase of the beam diameter at the end of the slowing stage due to random walk. Although the effect of transverse heating is less pronounced for the heavy cesium atoms because of the $\sim m^{-3/4}$ dependence of $\Delta v_\perp$ ($v_S \sim v_{\mathrm{thermal}}$), the resulting beam properties are unacceptable for our experiments in atom optics, and a reduction of the beam diameter combined with a transverse collimation is necessary. In addition, to eliminate the flux of unslowed atoms the slow atomic beam has to be deflected out of the axis of the cooling laser beam.

A magneto-optical deflection stage, as described by Scholz *et al.* [17] for Ne*, is one possibility to account for all requirements. However, the high mass of cesium together with the resonance wavelength of 852 nm leads to significant experimental problems. The position damping time of cesium in a 2D MOT is on the order of a few ms, which would require impracticable interaction lengths on the order of 10 cm for such a device. Therefore, we have employed a scheme which separates the positional from the velocity damping process. Hoogerland *et al.* [18] applied a similar scheme for the transverse collimation and compression of a supersonic Ne* beam using a 2D MOT as a lens for the atomic beam.

We use a magnetic hexapole lens made from permanent magnets [19] to focus the slow atomic beam into a 2D optical molasses tilted by 3 ° with respect to the slowing axis (Fig. 6). The magnetic lens with an inner diameter of 15 mm is assembled from 12 homogenously magnetized pie-shaped NdFeB segments ($B_R=1.2$ T). For cesium atoms in the $F=4, m_F=4$ ground state with $\mu=\mu_B$, the focal length is given by $f=\beta v^2$ with $\beta=2.1\times 10^{-5}$ s^2/m. The lens is located 200 mm past the end of the slowing stage and its distance to the beginning of the molasses region is 75 mm. The 2D molasses is formed by four mirrors glued to an aluminum frame in such a way as to recirculate a single incoming beam [20] [see Fig. 6(b)]. The light polarization is chosen to result

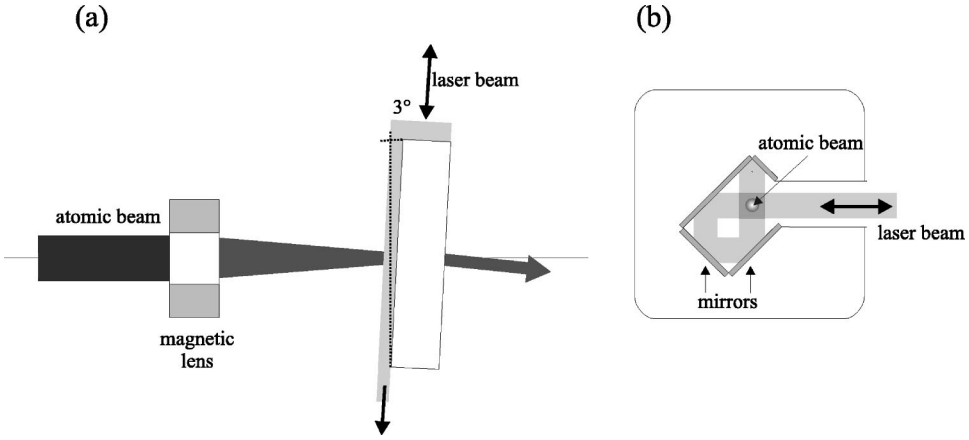

FIG. 6. Setup of the compression and deflection stage. (a) A magnetic hexapole lens focuses the slow atomic beam into the tilted optical collimation module. (b) Side view of the collimation module.

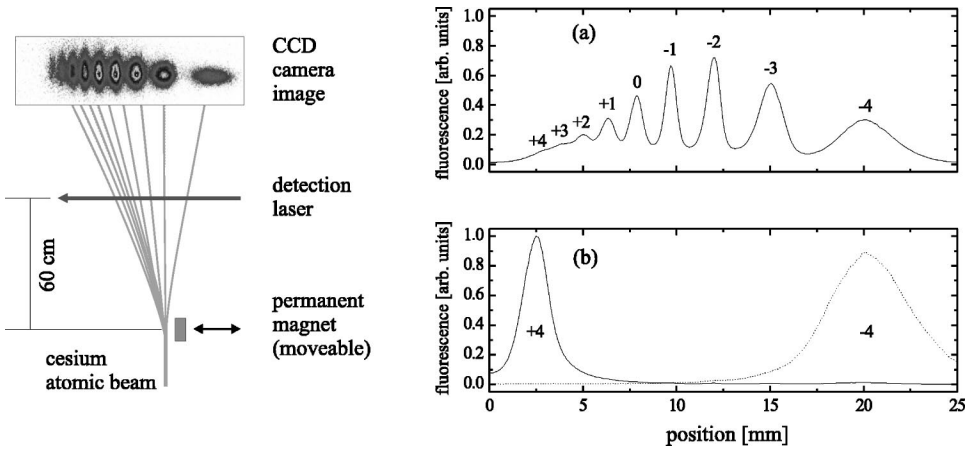

FIG. 7. A Stern-Gerlach setup with optical detection is used to determine the atomic distribution among the nine magnetic sublevels of the cesium $F=4$ ground state. (a) Distribution without optical pumping resulting from the optical molasses light field in the collimation module. (b) Atomic distribution with optical pumping. Solid line: slow atoms polarized in the $m_F=+4$ state. Dotted line: atoms polarized in the $m_F=-4$ state.

in a lin. $\perp$ lin. configuration. A small portion of the incoming laser beam (5 mm) escapes the mirrors and is not back-reflected. It provides enough light force pressure to deflect atoms with a longitudinal velocity of less than 65 m/s by 3 °. We have mounted the aluminum frame to an optical mirror holder which has been motorized. By this means the axis of the collimation module and thus the direction of the outcoming beam can be adjusted during the experiment.

More than 98% of the atoms in the deflected beam are in the $F=4$ ground state; however, the distribution among the nine m_F states is governed by the light field in the deflection zone. For atom optical experiments with magnetic components a beam entirely prepared in the $(F=4,m_F=4)$ state is desirable, because the effective magnetic moment of this state is independent of the magnetic field ($\mu=\mu_B$). Therefore the population has to be transferred to the $m_F=4$ state by optical pumping. This is done in a polarizing section about 40 cm downstream from the deflection zone, which is shielded from earth and stray magnetic fields with a cylindrical μ-metal shielding. The atomic beam enters and leaves the shielded region through two diametrical openings with 10-mm diameter. Two coils in a Helmholtz configuration provide a small and homogenous magnetic field of 10 μT inside the shielding. The direction of the magnetic field and therefore the quantization axis is perpendicular to the atomic beam axis. Two weak laser beams with a separation of 2 mm, circularly polarized and resonant with the $F=4\rightarrow F'=5$ transition, are sent along the symmetry axis of the magnetic field and optically pump the atoms into the $F=4,m_F=4$ state. This setup with two separated interaction zones was adopted from Ref. [21], and leads to a higher degree of polarization. To reduce the effect of laser light pressure on the atomic beam the laser beams are retroreflected.

The distribution of atoms among the ground state sublevels is detected using the Stern-Gerlach effect (Fig. 7). A few centimeters after the polarization setup a homogenously magnetized block of NdFeB with magnetic remanence $B_R=1.2$ T and a length of 2 cm mounted on a stage can be translated perpendicular to the atomic beam. Atoms in different magnetic substates are deflected by different angles, and the resulting spatial distribution is monitored via optical excitation and detection of the fluorescence with a charge-

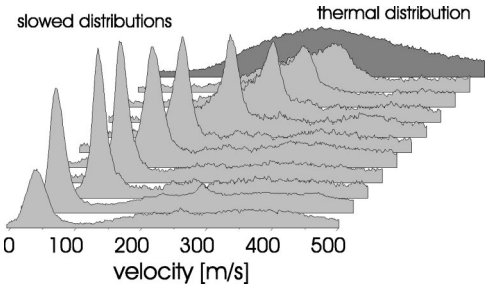

FIG. 8. Velocity distributions of the atomic flux density as measured by Doppler-sensitive fluorescence excitation. Cooling toward different longitudinal velocities is achieved by changing the detuning of the slowing laser from 270 MHz (front) to 50 MHz (back).

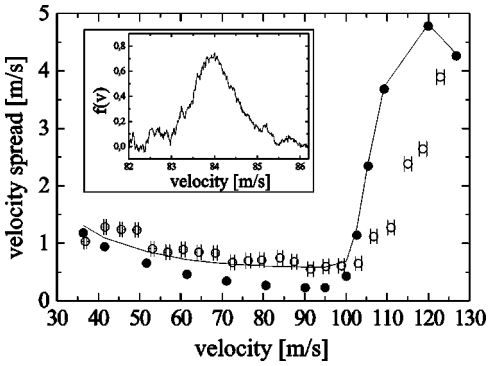

FIG. 9. The longitudinal velocity distribution is measured by a time-of-flight (TOF) technique. The values for $\Delta v_\parallel$ (open circles) are given as a function of the mean longitudinal velocity $\overline{v_\parallel}$ in comparison with the results of our numerical simulation (closed circles). The solid line includes experimental broadening mechanisms which have been quadratically added to the numerical results. Insert: Typical velocity distribution as calculated from a TOF signal.

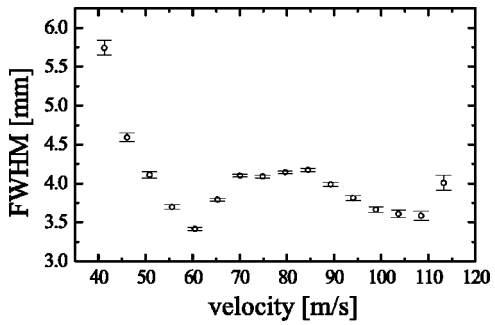

FIG. 10. Diameter (FWHM) of the slow atomic beam at a distance of 1.5 m behind the collimation and deflection stage.

coupled-device camera about 60 cm after the magnet. For atomic velocities less than 75 m/s the distribution can be spatially resolved completely. Figure 7(a) shows a CCD image of the split atomic beam together with a 1D cross section which clearly shows nine distinct peaks. With a 150-μm wide slit, we can select any of the nine atomic beams. Each of them is fully polarized in a single m_F state. Turning on the polarizing laser beam polarizes the atomic beam such that more than 97% of the atoms are in the $m_F=4$ state [the solid line in Fig. 7(b)]. By simply reversing the current through the coils or the handedness of the polarizing laser, respectively, the atoms are pumped into the $m_F=-4$ state [the dotted line in Fig. 7(b)].

IV. BEAM PROPERTIES

A. Longitudinal velocity distribution

A measurement of the longitudinal velocity distribution by Doppler-sensitive laser excitation is limited by the saturation-broadened natural linewidth Γ' of the excited state and the angle θ between atomic beam and laser beam to $\Delta v_{\parallel}=\Gamma'/k\cdot\cos\theta\geqslant\Gamma/k=4.5$ m/s. Nevertheless, for illustrating purposes Fig. 8 shows typical velocity distributions of the slowed atomic beam obtained with this method. Depending on the detuning of the slowing laser with respect to the undisturbed $F=4\rightarrow F'=5$ transition, the final atomic velocity distribution is narrowed and shifted toward central velocities between 35 and 120 m/s.

To enhance the velocity resolution we use a time-of-flight (TOF) technique on the deflected atomic beam [10]. A laser beam resonant with the $F=4\rightarrow F'=4$ transition is periodically turned on and off by a fast shutter (risetime <10 μs). This laser efficiently (~ 2 fluorescence cycles) pumps all the atoms into the $F=3$ ground state. These atoms are no longer resonant with a probe laser tuned to the $F=4\rightarrow F'=5$ transition which crosses the atomic beam under 90° in the detection region which is at a distance of $L=1.34$ m downstream from the ''chopping'' laser. A photomultiplier monitors the atomic fluorescence in the detection region. The velocity resolution of this TOF-measurement is given by $\Delta v_{\parallel}=-(v^2/L)\Delta t$, where $\Delta t=30$ μs is dominated by the time constant of the photomultiplier tube. For a longitudinal velocity of 100 m/s the velocity resolution is $\Delta v_{\parallel}\approx 0.2$ m/s, whereas for 40 m/s $\Delta v_{\parallel}$ is reduced to 3.6 mm/s, approaching the recoil velocity for cesium.

We have measured $\Delta v_{\parallel}$ for different longitudinal velocities, the result is shown in Fig. 9. The minimum width of $\Delta v_{\parallel}=0.55$ m/s is achieved for $v_{\parallel}=90$ m/s, where also the highest atomic current is produced (compare Fig. 12). For comparison, the results of our simulation (Sec. V) plus experimental broadening mechanisms, which have been quadratically added to the simulated data points, are plotted together with the measured data and show good agreement. The main broadening mechanisms, which are not included in our simulation, are the linewidth of the slowing laser (0.5 m/s) and longitudinal heating within the transverse cooling and deflection stage (0.14 m/s for $v_{\parallel}=90$ m/s). The radial variation of the magnetic flux density over the atomic beam diameter in the region where the slowing process stops has been measured with a Hall probe to be smaller than 10 μT, which results in an estimated broadening of the velocity distribution by 0.12 m/s.

B. Transverse beam properties

The slow atomic beam is analyzed at a distance of 1.5 m beyond the collimation and deflection stage, where it traverses a sheet of resonant laser light and the fluorescence is monitored with a CCD camera. In Fig. 10 we show the beam diameter in the detection region as a function of the longitudinal velocity. The variation is well understood as a

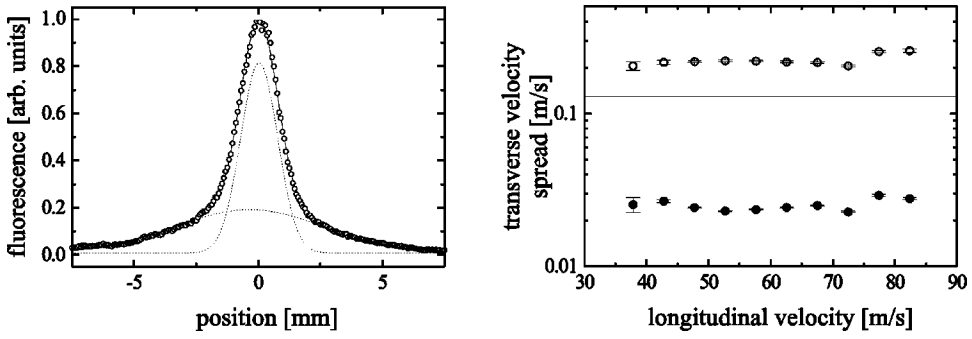

FIG. 11. Measurement of the transverse velocity spread of the atomic beam. (a) CCD fluorescence profile (open circles) fitted with the sum (solid line) of two Gaussian profiles (dashed lines). (b) Transverse velocity spread deduced from the two Gaussian profile components as a function of the longitudinal velocity. The horizontal line corresponds to the Doppler velocity limit for cesium atoms.

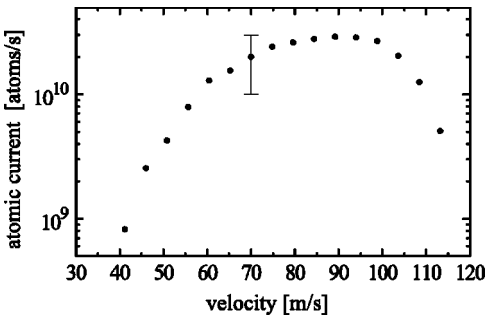

FIG. 12. Slow atomic beam current as a function of the longitudinal velocity.

combination of focusing properties of the magnetic hexapole lens (at $v_{\parallel}=60$ m/s the focal length of the hexapole lens coincides exactly with the distance between the lens and the beginning of the collimation zone) and a reduced transverse spreading toward higher longitudinal velocities.

To analyze the transverse velocity spread of the slow atomic beam, a movable narrow slit ($d=750$ μm) is inserted onto the atomic beam axis at a distance of 0.5 m behind the collimation stage. The atomic beam profiles in the detection region can be described as a sum of two different Gaussian profiles [Fig. 11(a)]. The width of one component is consistent with the Doppler limit for cesium, while the smaller one has to be associated with atoms transversely cooled to sub-Doppler temperatures [Fig. 11(b)].

C. Beam current

An interesting number when doing atom lithography is the total atomic current available. We have made absorption measurements on the slowed atomic beam which are presented in Fig. 12. The maximum values for brightness and brilliance are achieved with a longitudinal velocity of $v_{\parallel}=80$ m/s: $\mathcal{R}=6.3\times10^{21}$ atoms s^{-1} m^2 sr and $\mathcal{B}=7\times10^{23}$ atoms s^{-1} m^2 sr. Note that without the optical transverse collimation stage in the oven chamber the number of slow atoms in the deflected beam is reduced by a factor of about 20. Due to the large transverse velocity spread of the thermal atomic beam without optical collimation, only a small portion of the atoms is efficiently slowed and deflected.

The atomic current is currently limited by the oven design. A higher oven temperature leads to a decrease in atomic flux due to the buildup of vapor pressure in the oven chamber. With an improved setup we expect an increase in atomic current by one order of magnitude.

V. SIMULATION OF THE SLOWING PROCESS

For a better understanding of the slowing process we have performed a numerical simulation taking into account the longitudinal and transverse laser beam profile, the axial variation of the magnetic field as calculated from the known dimensions of the windings, and the randomness of absorption and spontaneous emission. Figure 13(a) shows the trajectory of an atom starting with a velocity of 270 m/s.

These simulations clearly show that the outcoming velocity distribution is mainly determined by the shape of the magnetic field at the end of the slowing stage. Figure 13 furthermore shows a comparison of three simulated velocity distributions: (b) during the slowing process at $z=1.20$ m, (c) after the atoms have left the slower without an additional steep gradient at the end, and (d) with permanent magnets applied at the end. The distribution without the permanent magnets becomes significantly broadened, as expected, whereas with permanent magnets applied the heating is drastically reduced, leading to a much smaller broadening effect (see Sec. II). There is a slight asymmetry in the longitudinal velocity distribution, which is also present in the TOF measurements (see the inset of Fig. 9). Molenaar *et al.* pointed out that the transverse beam profile of the slowing laser leads to additional broadening of the longitudinal velocity distribution [10]. We could confirm their findings by changing the shape of the slowing light field in the simulation to a plane wave. The resulting longitudinal velocity distribution in this case is Gaussian, and its width is reduced by roughly 30% although the variation of the laser intensity across the atomic beam at the end of the slowing stage in the experiment is less than 5%.

There are two reasons that explain the increase in the velocity width which occurs at about 100 m/s. First, there is an increase in the number of atoms in the thermal atomic beam with a velocity lower than the final velocity. Second, the shape of the magnetic field was optimized for velocities below 100 m/s.

SUMMARY

The Zeeman slowing technique is capable of producing slow and intense atomic beams. By carefully optimizing the termination of the slowing process we have achieved a slow cesium atomic beam with a narrow longitudinal velocity spread and a corresponding high brilliance. A numerical simulation of the slowing process was performed, and the results are in good agreement with the experimental data. This beam will be used for our experiments in atom optics and atom lithography.

ACKNOWLEDGMENTS

We wish to thank the BMBF, which financially supported this work under Contract No. 13N6636. Our special thanks go to H. Metcalf for many valuable discussions and for critically reading the manuscript.

APPENDIX

Several physical quantities have been introduced to provide a figure of merit for atomic beams. Generally, these quantities have been constructed in analogy to photometry [22], but seemingly no completely consistent set of definitions for atomic beams can be found in the literature. For instance, the designations ''brightness'' and ''brilliance'' are sometimes used without distinction. These quantities are related to the Liouville phase-space density

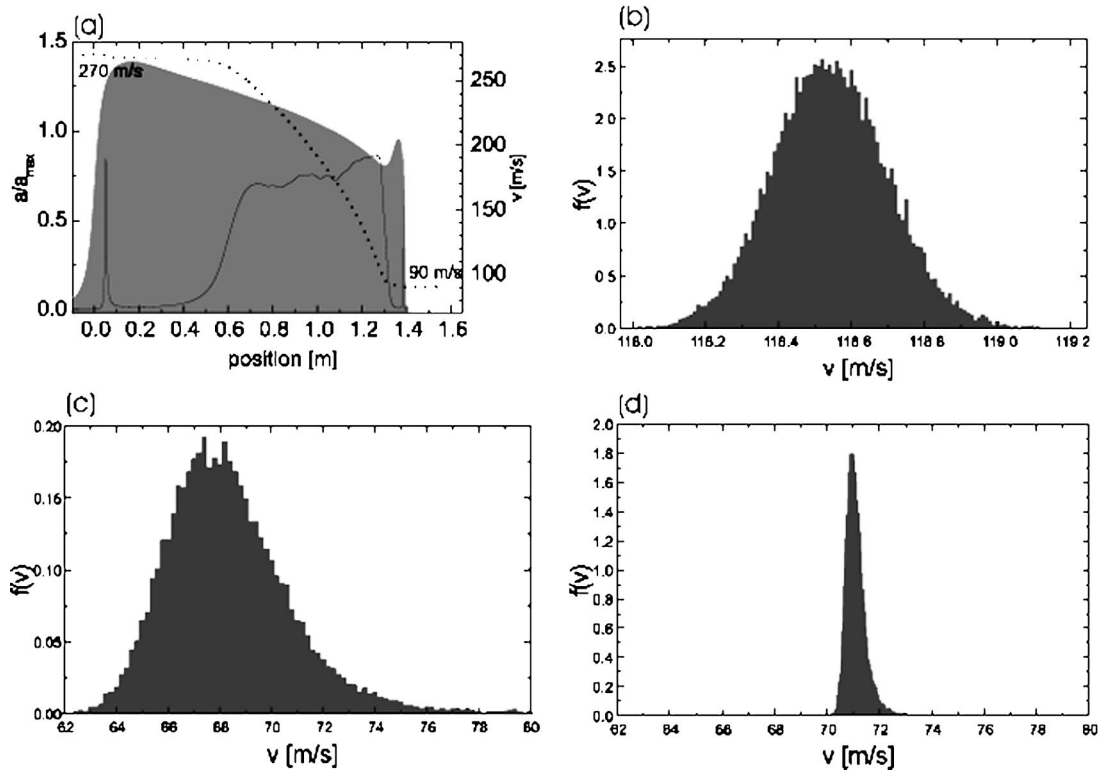

FIG. 13. Simulation of the slowing process. (a) Velocity (dotted line) and acceleration (solid line) of an atom starting at $v_{\parallel}=270$ m/s. The variation of the deceleration between $z=0.6$ and 1.3 m is due to imperfections of the magnetic field caused by the segmented coils. The shaded area shows the magnetic flux density. Longitudinal velocity distributions: (b) During the slowing process at $z=1.2$ m. (c) Outcoming velocity distribution without the steep gradient at the end of the Zeeman slower. (d) Velocity distribution with permanent magnets applied.

$$\Lambda=\frac{N}{(\Delta x\Delta p)^3}, \tag{A1}$$

which is the number of particles N per phase-space volume. Usually, in the context of atomic beams, axial and transverse motion of the atoms are not coupled. It is therefore natural to separate longitudinal ($\parallel$) from transverse ($\perp$) contributions to Λ. For circularly shaped atomic beams this leads to

$$\Lambda=\frac{1}{\pi(\Delta x_{\perp}\Delta p_{\perp})^2}\frac{N}{\Delta x_{\parallel}\Delta p_{\parallel}}. \tag{A2}$$

In the transverse direction the atoms occupy the phase-space volume $\pi(\Delta x_{\perp}\Delta p_{\perp})^2$. This quantity is, within a factor of π, equal to the emittance ϵ which is used to describe phase-space properties of particle accelerator beams [23]. The longitudinal contribution $N/(\Delta x_{\parallel}\Delta p_{\parallel})$ in Eq. (A2) is proportional to the longitudinal coherence length $\lambda_{coh}=h/\Delta p_{\parallel}$, and is easily expressed as $I/(\overline{v_{\parallel}}\Delta p_{\parallel})$ by introducing the average longitudinal beam velocity $\overline{v_{\parallel}}$ and the particle current $I=N\overline{v_{\parallel}}/\Delta x_{\parallel}$.

For calculating brightness and brilliance values from experimental data transverse and longitudinal coordinates are often mixed again via the solid angle $\Delta\Omega$, which in the paraxial approximation is expressed as $\Delta\Omega=\pi(\Delta p_{\perp}/\overline{p_{\parallel}})^2$. Hence, and for the sake of clarity, let us give explicit definitions for the *brightness* or *radiance*

$$\mathcal{R}=\frac{I}{\pi(\Delta x_{\perp})^2\Delta\Omega} \tag{A3}$$

and the *brilliance*

$$\mathcal{B}=\mathcal{R}\frac{\overline{p_{\parallel}}}{\Delta p_{\parallel}}, \tag{A4}$$

which is also called *spectral brightness* [23]. Note that for thermal atomic beams brightness and brilliance have similar values because $\overline{p_{\parallel}}/\Delta p_{\parallel}\simeq 1$. The *phase-space density* is then given by

$$\Lambda=\mathcal{B}\frac{\pi}{m^3\overline{v_{\parallel}^4}}, \tag{A5}$$

which is independent of the average longitudinal velocity $\overline{v_{\parallel}}$, as expected from its definition. The quantum limit occurs in accordance with the uncertainty relation if Λ is of order $1/h^3$ or larger, making h the natural physical unit and $\tilde{\Lambda}=\Lambda h^3$ a dimensionless quantity.

In our laboratory we are interested in the influence of atomic beam properties on imaging performance [19]. Two quantities of central interest are the point spread function and the chromatic aberrations, which are determined by beam divergence and chromaticity. The brilliance as defined by Eq. (A4) is a good measure of these properties.

[1] K. Dieckmann, R. J. C. Spreeuw, M. Weidemüller, and J. T. M. Walraven, Phys. Rev. A **58**, 3891 (1998).
[2] W. D. Phillips and H. Metcalf, Phys. Rev. Lett. **48**, 596 (1982).
[3] V. I. Balykin, V. S. Letokhov, V. G. Minogin, Yu. V. Rozhdestvensky, and A. I. Sidorov, J. Opt. Soc. Am. B **2**, 1776 (1985).
[4] M. A. Joffe, W. Ketterle, A. Martin, and D. E. Pritchard, J. Opt. Soc. Am. B **10**, 2257 (1993).
[5] E. Riis, D. S. Weis, K. A. Moler, and S. Chu, Phys. Rev. Lett. **64**, 1658 (1990).
[6] J. Nellesen, J. Werner, and W. Ertmer, Opt. Commun. **78**, 300 (1990).
[7] W. Ertmer, R. Blatt, J. L. Hall, and M. Zhu, Phys. Rev. Lett. **54**, 996 (1985).
[8] Z. T. Lu, K. L. Corwin, M. J. Renn, M. H. Anderson, E. A. Cornell, and C. E. Wieman, Phys. Rev. Lett. **77**, 3331 (1996).
[9] V. S. Bagnato, A. Aspect, and S. C. Zilio, Opt. Commun. **72**, 76 (1989).
[10] P. A. Molenaar, P. van der Straten, H. G. M. Heideman, and H. Metcalf, Phys. Rev. A **55**, 605 (1997).
[11] T. E. Barrett, S. W. Dapore-Schwartz, M. D. Ray, and G. P. Lafyatis, Phys. Rev. Lett. **67**, 3483 (1991).
[12] L. Ricci, M. Weidemüller, T. Esslinger, A. Hemmerich, C. Zimmermann, V. Vuletic, W. König, and T. Hänsch, Opt. Commun. **117**, 541 (1995).
[13] D. S. Weiss, E. Riis, Y. Shevy, P. J. Ungar, and S. Chu, J. Opt. Soc. Am. B **6**, 2072 (1989).
[14] P. D. Lett, W. D. Phillips, S. L. Rolston, C. E. Tanner, R. N. Watts, and C. I. Westbrook, J. Opt. Soc. Am. B **6**, 2084 (1989).
[15] J. Dalibard and C. Cohen-Tannoudji, J. Opt. Soc. Am. B **6**, 2023 (1989).
[16] H. R. Telle and H. Li, Electron. Lett. **26**, 858 (1990).
[17] A. Scholz, M. Christ, D. Doll, J. Ludwig, and W. Ertmer, Opt. Commun. **111**, 155 (1994).
[18] M. D. Hoogerland, J. P. J. Driessen, E. J. D. Vredenbregt, H. J. L. Megens, M. P. Schuwer, H. C. W. Beijerinck, and K. A. H. van Leeuwen, Appl. Phys. B: Photophys. Laser Chem. **62**, 323 (1996).
[19] W. G. Kaenders, F. Lison, I. Müller, A. Richter, R. Wynands, and D. Meschede, Phys. Rev. A **54**, 5067 (1996).
[20] M. D. Hoogerland, Ph.D. thesis, Technical University Eindhoven, 1993.
[21] B. P. Masterson, C. Tanner, H. Patrick, and C. E. Wieman, Phys. Rev. A **47**, 2139 (1993).
[22] See, e.g., L. Mandel and E. Wolf, *Optical Coherence and Quantum Optics* (Cambridge University Press, Cambridge, 1995).
[23] H. Wiedemann, *Particle Accelerator Physics* (Springer, Berlin, 1993).
[24] M. Schiffer, M. Christ, G. Wokurka, and W. Ertmer, Opt. Commun. **134**, 423 (1997).
[25] W. Rooijakkers, W. Hogervorst, and W. Vassen, Opt. Commun. **123**, 321 (1996).
[26] M. D. Hoogerland, D. Milic, W. Lu, H.-A. Bachor, K. G. H. Baldwin, and S. J. Buckman, Aust. J. Phys. **49**, 567 (1996); and (private communication).